STM JOURNALS

Journal of
Polymer & Composites

ISSN: 2321-2810 (Online)
ISSN: 2321-8525 (Print)
Volume 11, Special Issue 11, 2023
DOI (Journal): 10.37591/JoPC

http://engineeringjournals.stmjournals.in/index.php/JoPC/index

Research JoPC

# Optimization of Liquid Metal Nanocomposites and Biogas Addition Rate Using ANN-GA

S. Lalhriatpuia[1], Neeraj Budhraja[2,*], Kiran Pal[3]

***Abstract***

*In this study, the liquid metal nanocomposites were investigated using artificial neural network (ANN) prediction capabilities for Compression Ignition (CI) engine performance. The independent input variables selected were load (20-100%), Liquid-metal nanocomposites Doped Rate (NDR, 0-50 ppm), and Biogas Flow Rate (BFR, 0.5-1.0 kg/h). The Central Composite Face-Centered Design (CCFCD) was used in conjunction with the selected input variables and output parameters to assist in the preparation of the Design of Experiment (DOE). The proportion of error for the ANN projected output responses is determined for each run in the DOE. ANN model's predictions exhibited a good coefficient of determination ($R^2$), minimal Root Mean Square error (RMSE), and low Mean Absolute deviation (MAD), indicating accurate and reliable prediction capability. A response that was optimum according to the ANN model's optimization occurred at 74.5% load, 10.55 ppm NDR, and 0.656 kg/h BFR. The optimization response concludes that combining Liquid-metal nanocomposites and biogas contributes positively to diesel engine performances.*

**Keywords:** ANN, Nanocomposites, Biogas, Performance, Emission

## INTRODUCTION

With our overreliance on a finite supply of fossil fuels and ever-increasing energy demand over the recent decades, there is mounting alarm regarding the future availability of energy sources. Also, the emission generated via the utilization of these energy sources has been a significant concern given how the earth is shaping up in the form of climate change [1]. Hence, the requirement arises to investigate alternative renewable fuels to meet future demands. Some alternative renewable fuels explored are biodiesels, bio alcohols, biogas, etc. [2]. For the uses of biogas in CI engines, the techniques that exist today are either in the form of a Homogenous Charge Compression Engine (HCCI) or via dual fuel mode. The low cetane value of biogas gives it a disadvantage of high self-ignition temperature, which results in the need for higher cetane fuel to ignite biogas [3]. This disadvantage is suitably countered by the dual fueling of biogas with diesel. The external installation of a gas mixer is required in dual fuel operation to feed the biogas-air mixture through the input manifold.

***Author for Correspondence**
Neeraj Budhraja

[1,2]Research Scholar, Department of Mechanical Engineering, Delhi Technological University, Delhi, India
[3]Assistant Professor, Department of Mathematics, DITE DSEU Okhla Campus II, Delhi Skill & Entrepreneurship, Delhi, India

Received Date: December 01, 2023
Accepted Date: January 04, 2024
Published Date: February 23, 2024

**Citation:** S. Lalhriatpuia, Neeraj Budhraja, Kiran Pal. Optimization of Liquid Metal Nanocomposites and Biogas Addition Rate Using ANN-GA. Journal of Polymer & Composites. 2023; 11(Special Issue 11): S12–S27.

A study of dual-fueling biogas with diesel in a CI engine found a 6.1% reduction in BTE while increasing CO and HC emissions. In addition, the investigation shows an improvement in $NO_X$ and smoke emissions. The reduction in BTE is attributed to a drop in volumetric efficiency due to some air substituted by biogas. The less $NO_X$ could be attributed to $CO_2$ availability in biogas with high molar-specific heat, leading to lower combustion temperature. Also, methane concentration in biogas is reported to have a positive effect in inhibiting smoke formation [4].

 

A reduction of BTE, an increase in BSFC, an improvement in $NO_X$ and smoke emissions, and an increase in CO and HC were reported by other studies using biogas with diesel in CI engines [5, 6]. An investigation of the influence of load on dual fuel operating in CI engines reports a decline of BTE for dual fuel mode by 10% in low loads. However, the study concluded that at higher loads, the BTE gap between the diesel and dual fuel modes is narrowed [7]. Given our aim of lessening our dependence on diesel fuel, adding biogas as dual fuel in CI engines could be a vital difference. A 70% methane content biogas resulted in a diesel replacement of up to 87.5%, according to a study conducted on CI engines [8]. An analysis of the influence of BFR (0-1.2 kg/h) on the performance of the CI engine observed higher BSEC for the biogas run in contrast to the neat diesel run. Decrements in Smoke and $NO_X$ by 49% and 39%, respectively, were observed for the engine run on a BFR of 0.9 kg/h compared to the neat diesel [9].

Recent developments have observed the use of nanoparticles as additives to enhance engine performance and reduction in emissions owing to shortened ignition delay factors, the consequence of nanoparticles' better ignition attributes. In addition to enhancing magnetic characteristics, nanoparticles' increased surface-to-volume ratio and larger surface areas could also enhance catalytic reactivity [10]. A study of adding Alumina nanoparticles with a size of 50 nm in diesel at NDR of 0.5 g/L and 1 g/L for use in the diesel engine reported increased BTE, lower $NO_X$, and HC due to improved combustion characteristics [11]. A study of Alumina ($Al_2O_3$) fed to diesel at NDR of 25-100 ppm in CI engines revealed smoke emissions decline and combustion efficiency increment [12]. Copper oxide (CuO) nanoparticles fed at the rate of 0.5% (wt./wt.) to diesel for CI engine use were studied. An increment and decline of 4% and 4% for BTE and BSFC, respectively, were reported as opposed to a neat diesel run due to enhanced fuel characteristics in the form of flash point and heating value [13]. A comparison investigation for the usage of Alumina 50 ppm and CuO, 50 ppm on the CI engine, observed an increment in BTE, a decline in BSFC, and engine emission for both nanoparticles compared to CI. However, among the nanoparticles compared, more reduction of BSFC was observed for CuO, and more reduction of CO, UHC, and $NO_X$ was observed for Alumina. Oxygenated additives' CuO properties resulted in increased combustion temperature further leading to higher $NO_X$ formation [14]. A comparative study of Manganese oxide (MnO) and CuO fed to diesel at a rate of 200 mg/L in a CI engine resulted in improved performance and emission reduction for both in comparison to diesel. However, superior BTE and reduction of CO, HC, and $NO_X$ by 4%, 37%, 1%, and 4%, respectively, were observed for the MnO-diesel blend [15]. An investigation of Titanium oxide ($TiO_2$) nanoparticles usage in the CI engine at the feed of 0.20% added with 99.8% diesel resulted in an increase in brake power and a decline in BSFC, $NO_X$, CO, and $CO_2$ because of metallic nanomaterial compounds' greater heating value and surface area [16]. Improvement in combustion characteristics and reduced soot production by 11% were reported for a study on $CeO_2$-diesel blend with the feed of 50-100 mg/L in a 4-cylinder CI engine. The substitution effect of oxygen in $CeO_2$ speeds up the diffusion and oxidation rate enhancing fuel combustion [17]. Nanocomposites research has increased because to the fascination with synthetically manipulating nanostructures. Nanocomposites' temperature, magnetic characteristics, and charge capacity depend on morphology and interfacial aspects. Nanoparticles and nanolayers' high surface area-to-volume and aspect ratio make them ideal for polymeric materials. These structures integrate basic component qualities to improve mechanical and superconducting properties, making them ideal for high-tech applications. This feature underpins hybrid nanocomposites' matrices. Nanocomposites increase mechanical characteristics. Gas permeability, electrical/thermal conductivity, hardness, modulus, dimensional stability, strengthening. Nanocomposites can be made using clay, polymers, carbon, and nanoparticles[18]. Nanocomposites made of liquid metal alloys are either suspended in a polymer matrix as nanoparticles or combined with metallic nanoparticles to form a biphasic composition in which the liquid metal is the continuous matrix phase. The possibility of liquid metal nanocomposites altering the electrical, dielectric, and thermal property tuning of materials is exciting. For percolation and electrical conductivity at high concentrations, using thicker materials increases stiffness and mechanical hysteresis. Though tolerable in many contexts, this compromise is impeding the

 

development of computer, robotic, and medical systems that will one day necessitate mechanical adherence to biological tissues and materials. Substituting liquid metal nanodroplets for stiff filler greatly increases the potential uses of nanocomposite materials [19].

The correlation of input and output parameters is predicted using ANN computational tools from experimental data. For optimization purposes, ANN-GA are cost-effective and time-saving solution [20]. Research on RSM in CI engines considers the quantity of alumina nanoparticles NDR (40-160 ppm) and engine speed (800-1000 rpm) as input factors and BP, torque, BSFC, CO, HC, $CO_2$, and NOx as its output parameters. The study observed an optimum value of output parameters for nanoparticles blend NDR at 160 ppm and 1000 rpm engine speed [21]. An RSM study in the CI engine was carried out with CR (16 to 18), Load (20 to 100%), BFR (1.2 to 3.2 kg/h) as the input variables, and BTE, smoke, CO, HC, and $NO_X$ as the dependent output response. RSM optimization with desirability observed optimal performance and emission response at 80% load, 18 CR, and 2.8 kg/h BFR [22].

**Motivation and Novelty in Objectives**

Over-dependence on the limited supply of fossil fuel with the burden of emission as a consequence of its utilization has been a major concern. The literature survey suggests that biogas, without enrichment, can potentially substitute up to 87.5% diesel when used as dual fuel [8]. The literature survey showed adding nanoparticles to diesel has improved engine performance and emission [15–17, 21, 22]. No research has been conducted on optimising the combined addition rate of Liquid-metal nanocomposites and biogas in diesel engines. The input factors of load, Liquid-metal nanocomposites doped rate (NDR), and Biogas Flow Rate (BFR) are optimised for their impact on engine performance responses utilizing the developed ANN models.

## MATERIALS AND METHODS

**Nanoparticles Properties**

The NiO was sourced from Sigma Aldrich. A Zeiss scanning electron microscope (SEM) EVO 50 is used to determine the morphological structure of the nanoparticles. The SEM image indicates very densely, non-uniform, larger agglomerated particles, the shape mainly spherical and oval. The agglomeration factor is because of the NiO nanoparticles' high surface energy and surface tension [10]. Figure 1 SEM image pictures prove the nanoparticles are less than 100 nm on average.

NiO nanoparticle elemental composition is determined using the RONTEC EDX system model Quantax 200. Ni and O are confirmed to be present in Figure 2, and no peak detection of foreign elements suggests the nanoparticles utilized are very pure. The observation of Ni and O atomic percentages of 49.77% and 50.23%, respectively, further confirms the 1:1 NiO theoretical ratio. The elemental mapping images in Figure 3 indicate an equal ratio of Ni and O elements in the lattice.

**Liquid metal Nanocomposites Blend Preparation and Properties**

For one hour, diesel and nanoparticles were mixed in an ultrasonication bath to form Liquid-metal nanocomposites at concentrations of 25 ppm and 50 ppm, respectively. After that, for 30 minutes, the mixture is mixed again with the use of an ultrasonicator probe operating at 50 Hz. 1% Triton X-100 surfactant by weight was added to avoid agglomeration due to surface tension. After observing the blends for 24 hours, no agglomeration or settlings of particles were observed in the fuel blend. As mentioned in Table 1, the properties of the pilot fuels used in the study were then measured utilizing several ASTM testing methods.

**Biogas Properties**

The biogas composition changes based on feedstock and production parameters; carbon dioxide and methane are the two primary components. Also, there are hydrogen sulfide ($H_2S$) remains in their unprocessed state. In this research, biogas was generated using food waste as its main ingredient. To

 

remove $H_2S$, the raw biogas was put through a medium consisting of iron sponges. Table 2 displays the calorific value and ultimate gas composition. A biogas analyzer is used to test the biogas composition, while a Junker's calorimeter is used to determine the calorific value.

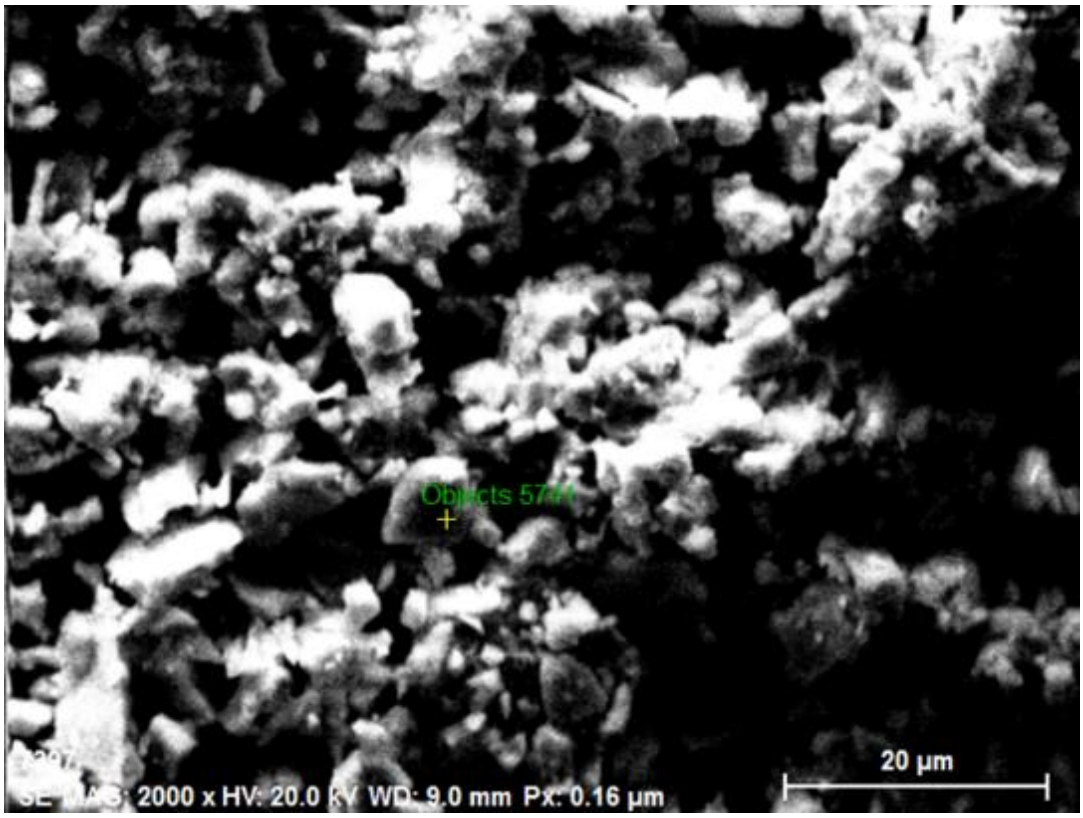


**Figure 1.** EDX spectra of NiO nanoparticles.

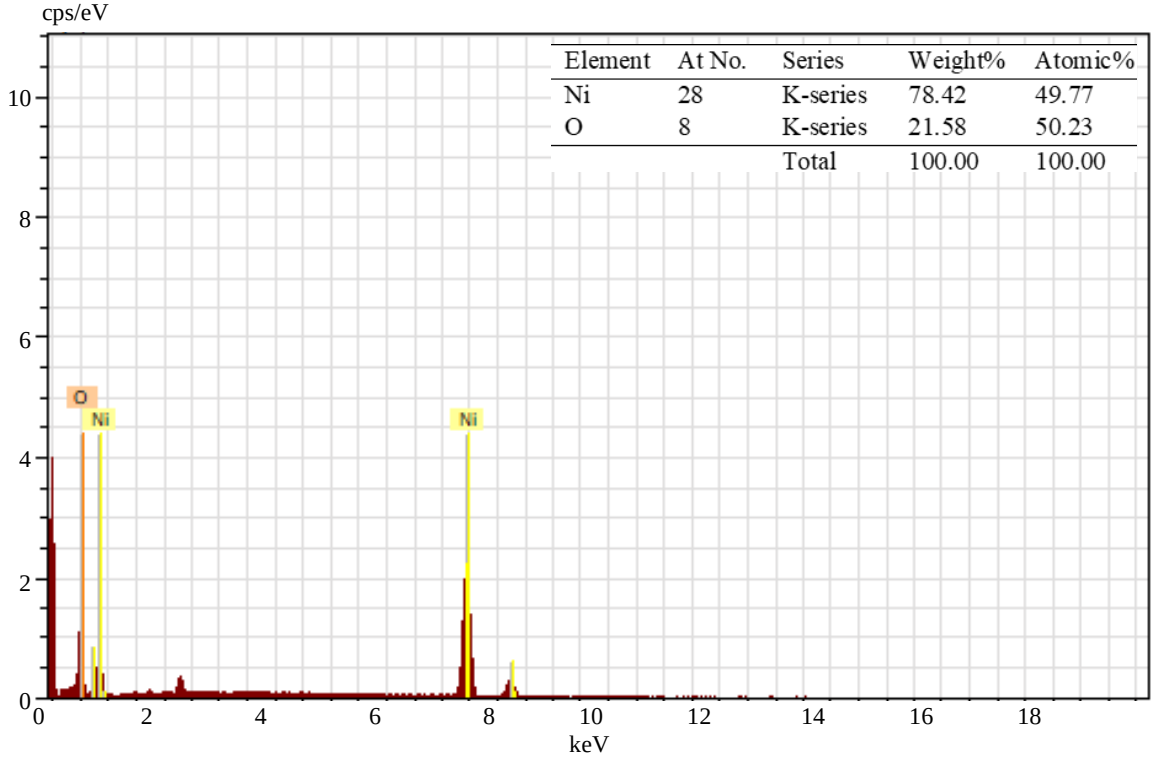


**Figure 2.** SEM images of NiO at 30 µm.

 

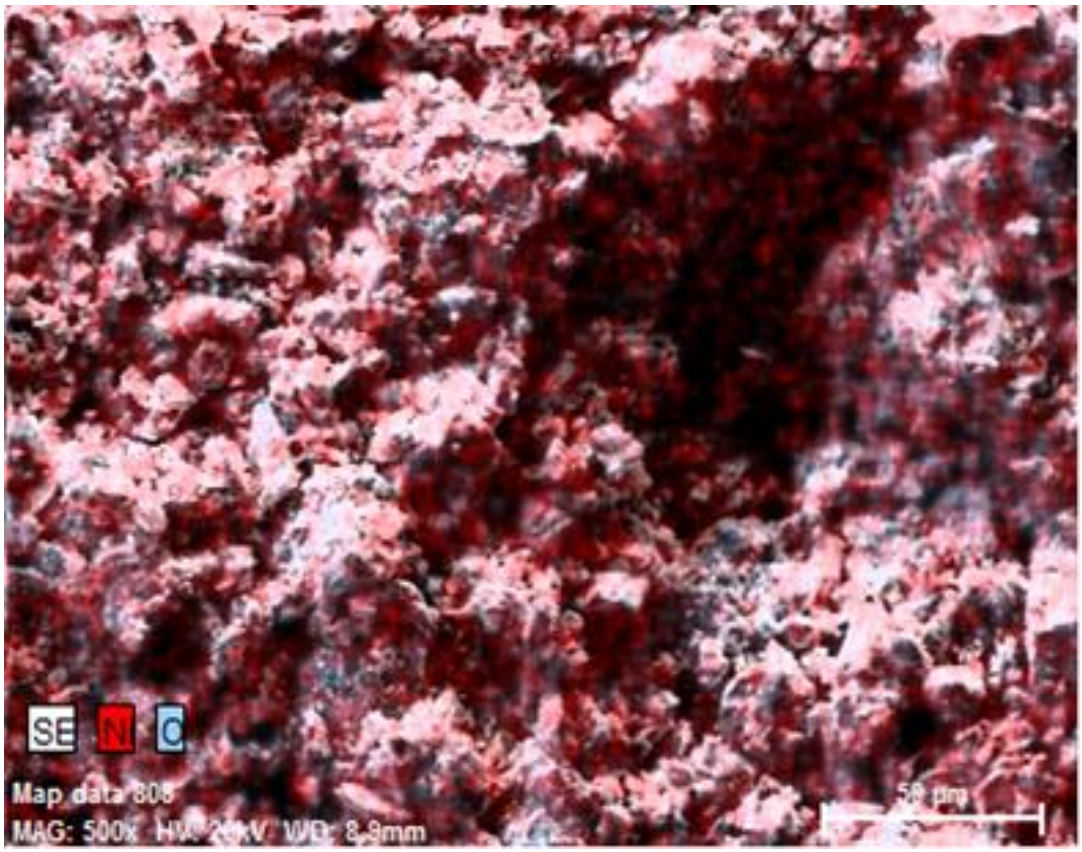


**(a) NiO**

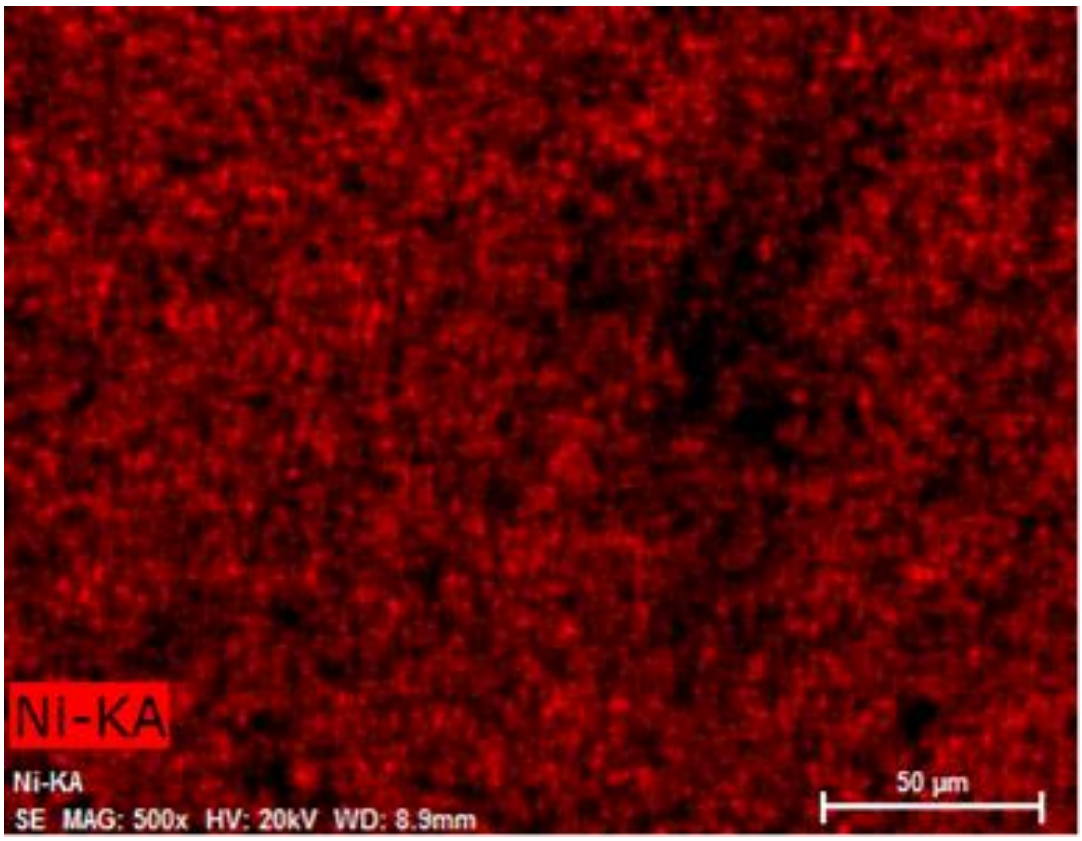


**(b) Ni**

 

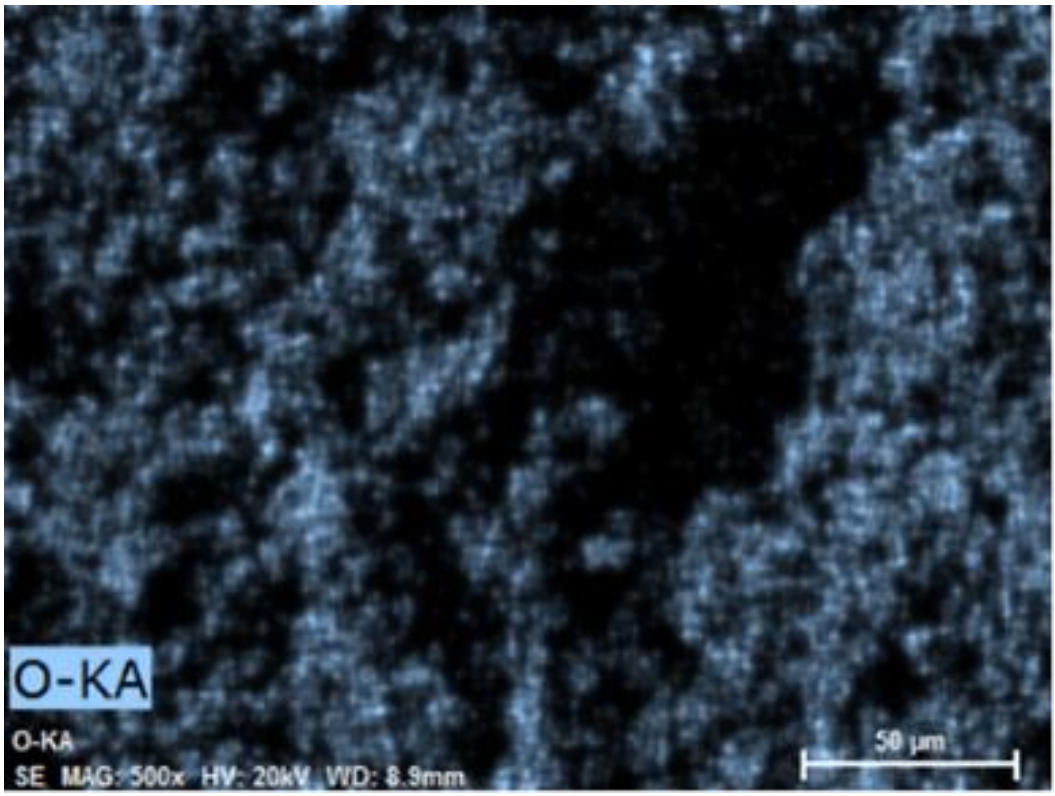


**(c) O**

**Figure 3.** Elemental mapping of (a) NiO, (b) Ni, and (c) O.

**Table 1.** Physicochemical properties of test fuels.

| Properties | Unit | Testing methods | Diesel | Diesel+NDR 25 ppm | Diesel+NDR 50 ppm |
|---|---|---|---|---|---|
| Kinematic Viscosity at 40°C | cSt | D-445 | 2.6 | 2.66 | 2.79 |
| Density at 40°C | $kg/m^3$ | D-1298 | 840 | 841.99 | 845.97 |
| Calorific Values | MJ/kg | D-240 | 43.2 | 43.25 | 43.36 |
| Flash Point | °C | D-93 | 69 | 67.29 | 66.44 |
| Pour Point | °C | D-97 | -8 | -8.32 | -8.48 |
| Cetane Number | - | D-4737 | 48 | 48.91 | 49.15 |

**Table 2.** Biogas Composition.

| Properties | Unit | Value |
|---|---|---|
| $CH_4$ | % | 68 |
| $CO_2$ | % | 25 |
| $H_2S$ | ppm | 2 |
| $O_2$ | % | 0.5 |
| Calorific Value | MJ/kg | 26 |

## Experimental Setup and Methodology

The experiment used a CI engine with a single cylinder, four strokes, and a constant speed that had a rated output of 3.5 kW. For applying load, a dynamometer-type eddy current was used. In regards to this research, the load varies between 2.4 kg (20%) to 12 kg (100%). The water-cooled engine's flow was monitored with rotameters. A manometer and a fuel measuring unit are used to measure airflow and fuel flow. Temperature sensors are positioned at various sites, and continuous data is collected using PT100 sensors. Connected to an NI unit, these sensors record data and transmit it to the

 

computer with EngineSoft software. A gas-air mixing mechanism is added to the arrangement to provide dual fuel operation. The data from engine specifications were used to construct the gas-air mixing system. The experimental setup and gas mixer utilized in the investigation are schematically shown in Figure 4 [23, 24].

A biogas flow meter (Siya SI 2.5) was used to assess the BFR, and the rate of flow modification was achieved through modulation in the ball valves. A gas analyzer (Make: AVL DiGas 480) was used to evaluate emissions, and a smoke meter (Make: AVL 437C) was used to quantify smoke opacity. The methodology process chart of this current study is given in Figure 5. The study conducted can be classified mainly into three stages as follows:

1. Fuel blend preparation and engine testing as per DOE
2. Characterization of fuels
3. Modelling and optimization using ANN-GA

**Artificial Neural Network Modelling**

Analytical tools like artificial neural networks (ANNs) mimic the way the brain works to validate correlations between input and output variables and to build data predictability regressions [25]. The model design Figure 6 shows the three-layered feed-forward back propagation neural network that was used. The input layer had three nodes: Load, NDR, and BFR. The hidden layer had ten neurons. The output layer had six nodes: BTE, BSEC, $NO_X$, HC, CO, and Smoke. The model was trained using MATLAB version R2020a. All layer contains neurons, and links are the connection made between the neurons. These links are then provided weights and bias so that the neurons can converse with each other. Levenberg-Marquardt (trainlm) was used for training, and gradient descent with momentum weight and bias (LEARNGDM) was used for adaptive learning. The performance function was a mean square error (MSE). The input and output layers used linear transfer functions, whereas the hidden layer used hyperbolic tangent sigmoidal (tansig) transfer functions. There are a total of 20 runs in the DOE. 14 runs, or 70% of the total, were utilized for network training. Three runs, or 15% of the whole, were then allocated for testing, and the remaining 15% were reserved for validation.

**Evaluation metrics and Validation**

There is an accuracy rate computed for each DOE run to evaluate the measurement mismatch between the actual data and the expected outcomes from the ANN using eq. (1). To evaluate the ANN model's prediction efficacy, we used $R^2$, RMSE, and MAD, which were computed using eq. (2), (3), and (4),

$$Percentage\ error = \frac{|\text{Observed result} - \text{Predicted result}|}{\text{Observed result}} \quad (1)$$

$$R^2 = 1 - \left(\frac{\sum_{t=1}^{n}(A_t - F_t)^2}{\sum_{t=1}^{n}(F_t)^2}\right) \quad (2)$$

$$RMSE = \sqrt{\frac{\sum_{t=1}^{n}(A_t - F_t)^2}{n}} \quad (3)$$

$$MAD = \frac{\sum_{t=1}^{n}|A_t - F_t|}{\text{n}} \quad (4)$$

$A_t$ denotes the observed data, Ft stands for the projected data, and n represents the total number of DOE runs.

To determine whether the result obtained via optimization is accurate, validation is required. The optimal values for the ANN model's input parameters are tested experimentally. Using eq. (1), we can determine the proportion of inaccuracy between the experimental data and the optimized response parameters predicted by the ANN models.

 

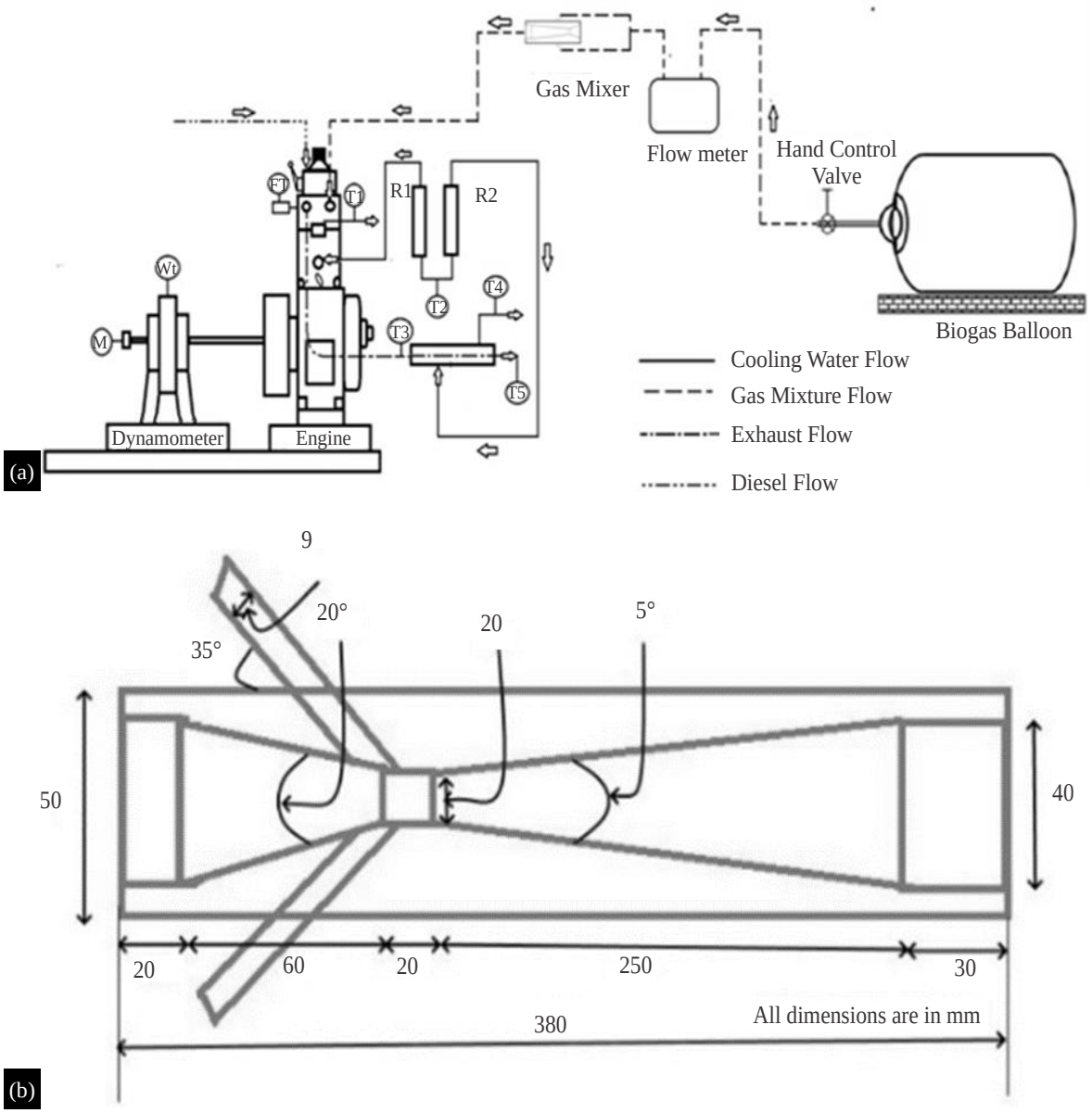


**Figure 4.** Schematic overview of (a) the experimental setup; and (b) gas mixer.

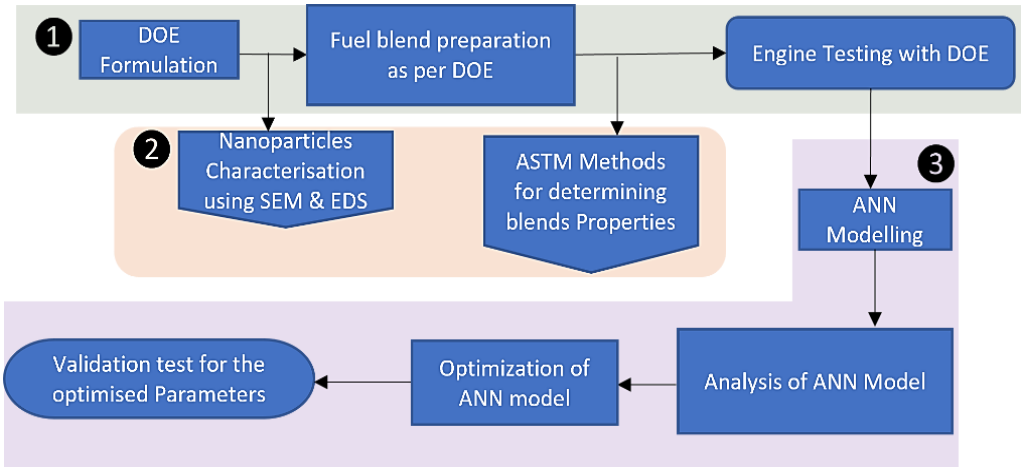


**Figure 5.** Methodology process chart.

 

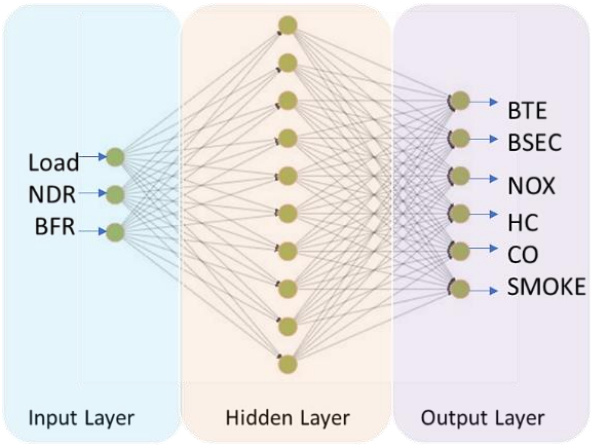


**Figure 6.** ANN Model architecture.

### GA Optimization for ANN

Evolutionary algorithms, such as GA, are a way to conduct research and exploration that is similar to the idea of natural selection. The GA fitness function is defined using the trained network that was constructed for each ANN model output response. An objective function, a fitness function takes as inputs the desired outcomes, which may be either maximizing or minimizing the responses. Table 3 contains the selection parameters, as well as the upper and lower limits of the input parameters, which are subsequently submitted to the GA programme. In GA optimization, there are five steps: initial population, fitness function, selection, crossover, and mutation. From the ANN-based objective function, GA grades and selects the solution [26].

## RESULTS AND DISCUSSIONS

### DOE Evaluation

The Central Composite Face-Centered Design (CCFCD) was used in conjunction with the selected input variables and output parameters to assist in the preparation of the DOE in the Design Expert Software. Data from DOE experiments' experimental runs are shown in Table 4.

### ANN Model Analysis

In order to determine the output parameters' correlation coefficient (R), a network was established for each step of the process (training, testing, and validation). Both Figure 7 and Figure 8 provide the total R-values for all dependent responses. A high R-value for any given network indicates that the DOE data was well-trained, which allows us to draw additional conclusions about the reliability of the regression model.

### Evaluated metrics of the ANN Model

The proportion of error for the ANN projected output responses is determined for each run in the DOE using eq. (1), as shown in Figure 9.

Table 5 displays the evaluation metrics for the ANN model's prediction: $R^2$, RMSE, and MAD. For the most part, the ANN model's predictions had good $R^2$, minimal RMSE, and low MAD. The ANN model's accurate predictions and minimal error rates prove that it is a trustworthy regression analysis for the input variables studied.

**Table 3.** Optimizing GA using Selection Parameters.

| Population Type | Initial Population | Mutation Rate | Crossover Fraction | Selection Function |
|---|---|---|---|---|
| Double Vector | 50 | 0.01 | 0.8 | Tournament |

 

**Table 4.** DOE and the results of experiments.

| Run | A:load | B:NDR | C:BFR | BTE | BSEC | $NO_x$ | HC | CO | SO |
|---|---|---|---|---|---|---|---|---|---|
| | *%* | *ppm* | *kg/h* | *%* | *MJ/kWh* | *ppm* | *ppm* | *%* | *%* |
| 1 | 60 | 25 | 0.75 | 15.89 | 22.36 | 204 | 46.05 | 0.091 | 29.21 |
| 2 | 100 | 0 | 0.5 | 21.63 | 19.52 | 450 | 42.68 | 0.1108 | 50.41 |
| 3 | 20 | 0 | 0.5 | 10.45 | 34.33 | 114 | 55.76 | 0.1496 | 18.93 |
| 4 | 60 | 25 | 0.75 | 16.1 | 22 | 202 | 45.05 | 0.09 | 28.91 |
| 5 | 20 | 50 | 1 | 9.29 | 38.73 | 77 | 57.05 | 0.1446 | 13.46 |
| 6 | 20 | 50 | 0.5 | 11.05 | 32.24 | 108 | 52.43 | 0.133 | 16.83 |
| 7 | 100 | 50 | 0.5 | 23.12 | 18.12 | 419 | 39.71 | 0.0952 | 44.86 |
| 8 | 60 | 0 | 0.75 | 14.86 | 24.07 | 229 | 50.06 | 0.103 | 30.75 |
| 9 | 100 | 25 | 0.75 | 21.21 | 19.79 | 348 | 41.12 | 0.1043 | 42.3 |
| 10 | 60 | 25 | 0.75 | 15.91 | 22.11 | 203 | 45.51 | 0.091 | 29.7 |
| 11 | 100 | 50 | 1 | 19.86 | 20.79 | 298 | 43.07 | 0.1060 | 35.89 |
| 12 | 60 | 50 | 0.75 | 16.34 | 21.66 | 199 | 44.97 | 0.089 | 27.36 |
| 13 | 20 | 25 | 0.75 | 10.44 | 36.22 | 80 | 54.97 | 0.1436 | 15.81 |
| 14 | 60 | 25 | 0.75 | 15.71 | 22.51 | 206 | 46.53 | 0.0917 | 29 |
| 15 | 60 | 25 | 0.75 | 15.76 | 22.42 | 205 | 46.21 | 0.091 | 29.5 |
| 16 | 60 | 25 | 0.75 | 16.12 | 21.55 | 200 | 44.53 | 0.091 | 29 |
| 17 | 60 | 25 | 0.5 | 16.82 | 21.03 | 255 | 45.87 | 0.086 | 33.16 |
| 18 | 60 | 25 | 1 | 14.63 | 25.16 | 180 | 49.28 | 0.097 | 26.34 |
| 19 | 20 | 0 | 1 | 8.67 | 41.64 | 83 | 62.22 | 0.1624 | 15.22 |
| 20 | 100 | 0 | 1 | 18.39 | 22.58 | 328 | 47.34 | 0.122 | 40.22 |

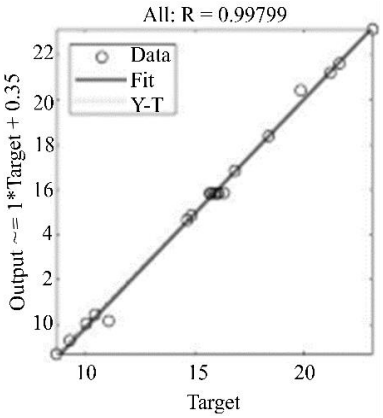


(a) R of BTE

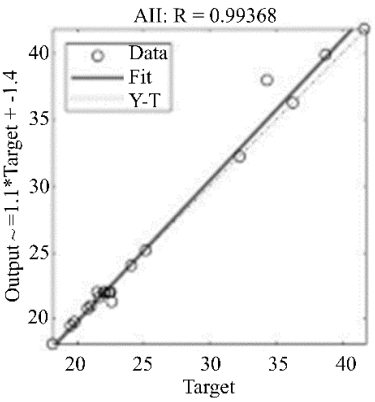


(b) R of BSEC

 

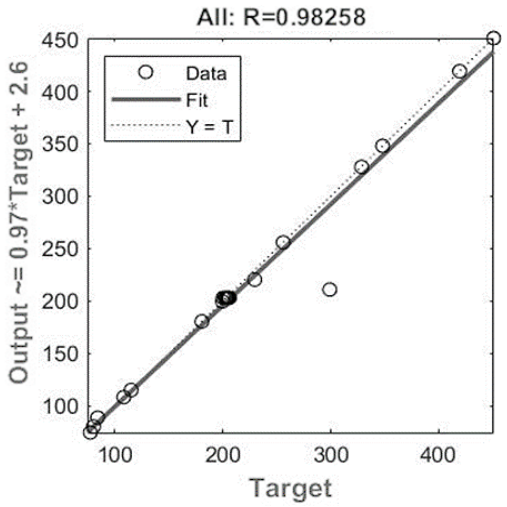


(c) R of $NO_x$

**Figure 7.** R for the trained network in for outputs (a) BTE, (b) BSEC, and (c) $NO_X$.

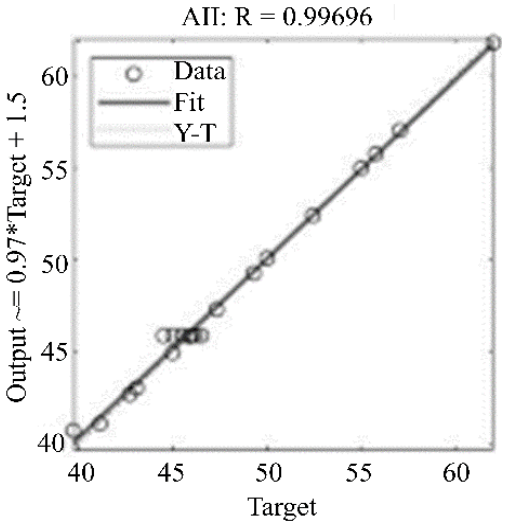


(d) R of HC

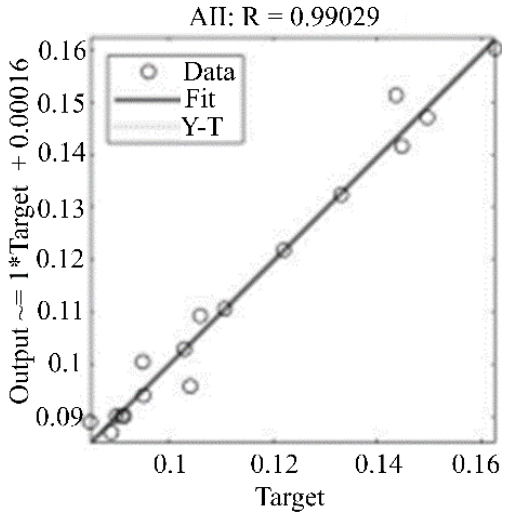


(e) R of CO

 

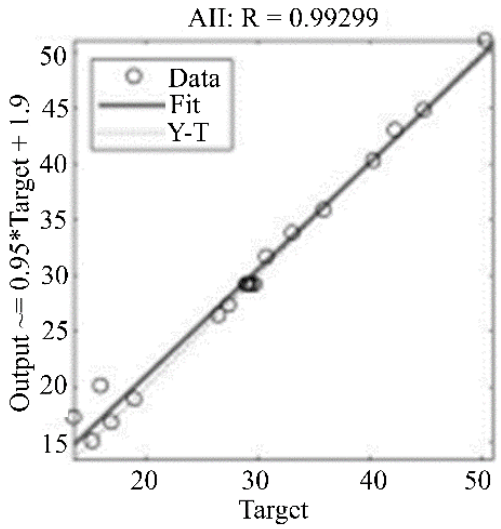


(f) R of Smoke

**Figure 8.** R for the trained network for outputs (d) HC, (e) CO, and (f) Smoke opacity.

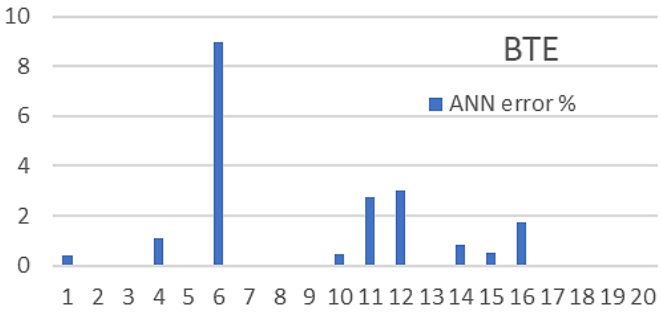


(a) BTE responses

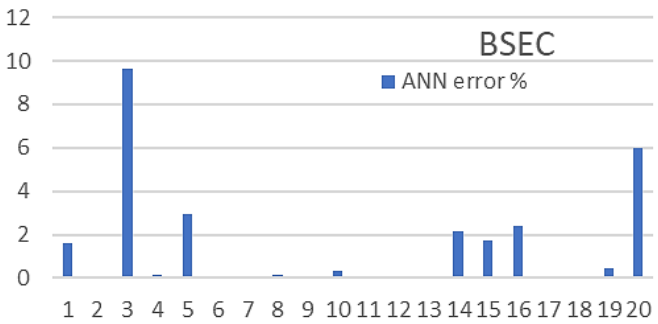


(b) BSEC responses

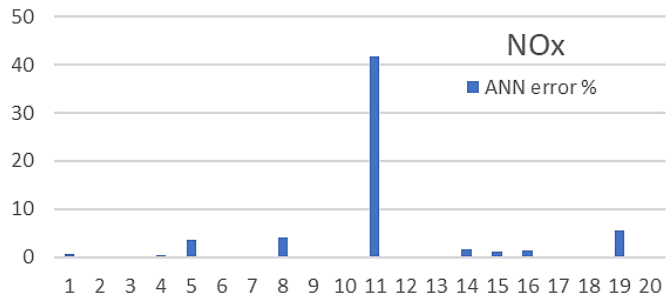


(c) NOx responses

 

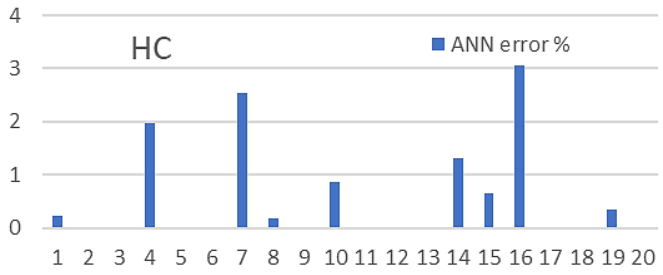


(d) HC responses

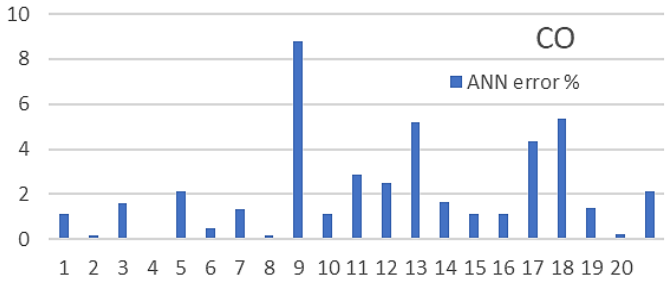


(e) CO responses

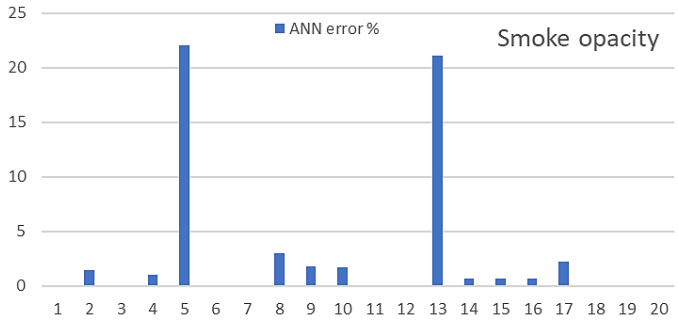


(f) Smoke opacity responses

**Figure 9.** Percentage in error for predicted engine performance and emission responses.

**Table 5.** Evaluation metrics for ANN Model Predictions.

| Outputs | $R^2$ | | RMSE | | MAD |
|---|---|---|---|---|---|
| BTE | 0.9959 | | 0.276 | | 0.137 |
| BSEC | 0.9873 | | 0.928 | | 0.411 |
| $NO_x$ | 0.9654 | | 19.873 | | 5.790 |
| HC | 0.9939 | | 0.475 | | 0.254 |
| CO | 0.9806 | | 0.003 | | 0.002 |
| Smoke opacity | 0.9860 | | 1.332 | | 0.632 |

**Optimization of input parameters and Validation**

At a load of 74.5%, NDR of 10.55 ppm, and BFR of 0.656 kg/h, the ANN-GA optimization method predicted an ideal value of BTE, BSEC, $NO_X$, HC, CO, and smoke opacity of 17.5%, 20.9 MJ/kWh, 330 ppm, 46 ppm, 0.098%, and 41.6%, respectively.

Table 6 displays the optimum predicted results, validation outcomes, and Errors. Results optimized by the model have a percentage error of less than 5%, which is deemed significant enough for acceptance.

 

**Table 6.** ANN-GA optimized parameter's validation test results and error percentage.

| Output | Model Technique: ANN-GA | | |
|---|---|---|---|
| | ***Experiment*** | ***Estimated*** | ***Errors (%)*** |
| BTE | 18.05 | 17.5 | 3.09 |
| BSEC | 21.47 | 20.9 | 2.69 |
| $NO_X$ | 321.15 | 330 | 2.72 |
| HC | 46.88 | 46 | 1.89 |
| CO | 0.103 | 0.098 | 3.15 |
| SO | 43.25 | 41.6 | 4.97 |

## CONCLUSIONS

Twenty experimental runs of CCFCD matrices were created for the DOE as part of this investigation. A model using ANN was constructed based on the DOE findings. The following are the key conclusions drawn from the study:

1. According to the criteria used for assessment, the ANN regression model performed effectively and had a low prediction error rate. The ANN model's predictions made were precise and dependable, with low RMSE and MAD and high $R^2$.
2. The ANN-GA model was optimized to achieve the following responses: 17.5% for BTE, 20.9 MJ/kWh for BSEC, 330 ppm for $NO_X$, 46 ppm for HC, 0.098% for CO, and 41.6% for smoke opacity, all with operational inputs of 74.5% load, 10.55 ppm NDR, and 0.656 kg/h BFR.
3. Optimal results from ANN models have shown to have low error percentages (less than 5%) in validation runs.

Considering the optimized results from the ANN model, it may be concluded the performance and emissions of CI engines are improved when biogas is combined with Liquid-metal nanocomposites. Investigating the impacts of load, NDR, and BFR on CI engines also reveals that ANN is a dependable and accurate tool.

**Acknowledgments**

The authors are thankful for all the support provided by the Delhi Technological University, Delhi, India.

## REFERENCES

1. Fathi M, Ganji DD, Jahanian O. Intake charge temperature effect on performance characteristics of direct injection low-temperature combustion engines. J Therm Anal Calorim. 2020; 139: 2447–2454. doi: 10.1007/s10973-019-08515-y.
2. Budhraja N, Pal A, Mishra RS. Parameter optimization for enhanced biodiesel yield from Linum usitatissimum oil through solar energy assistance. Biomass Convers Biorefin. 2022. doi: 10.1007/s13399-022-03649-w.
3. Barik D, Sivalingam M. Performance and Emission Characteristics of a Biogas Fueled DI Diesel Engine. SAE Technical Paper 2013-01-2507. 2013. doi: 10.4271/2013-01-2507.
4. Barik D, Murugan S. Experimental investigation on the behavior of a DI diesel engine fueled with raw biogas–diesel dual fuel at different injection timing. Journal of the Energy Institute. 2016; 89 (3): 373–388. doi: 10.1016/j.joei.2015.03.002.
5. Mahla SK, Singla V, Sandhu SS, Dhir A. Studies on biogas-fuelled compression ignition engine under dual fuel mode. Environmental Science and Pollution Research. 2018; 25: 9722–9729. doi: 10.1007/s11356-018-1247-4.
6. Aklouche FZ, Loubar K, Bentebbiche A, Awad S, Tazerout M. Experimental investigation of the equivalence ratio influence on combustion, performance and exhaust emissions of a dual fuel diesel engine operating on synthetic biogas fuel. Energy Convers Manag. 2017; 152: 291–299. doi: 10.1016/j.enconman.2017.09.050.

 

7. Swami Nathan S, Mallikarjuna JM, Ramesh A. An experimental study of the biogas–diesel HCCI mode of engine operation. Energy Convers Manag. 2010; 51 (7): 1347–1353. doi: 10.1016/j.enconman.2009.09.008.
8. Ambarita H. Performance and emission characteristics of a small diesel engine run in dual-fuel (diesel-biogas) mode. Case Studies in Thermal Engineering. 2017; 10: 179–191. doi: 10.1016/j.csite.2017.06.003.
9. Barik D, Murugan S. Investigation on combustion performance and emission characteristics of a DI (direct injection) diesel engine fueled with biogas–diesel in dual fuel mode. Energy. 2014; 72: 760–771. doi: 10.1016/j.energy.2014.05.106.
10. Paramashivaiah BM, Banapurmath NR, Rajashekhar CR, Khandal SV. Studies on Effect of Graphene Nanoparticles Addition in Different Levels with Simarouba Biodiesel and Diesel Blends on Performance, Combustion and Emission Characteristics of CI Engine. Arab J Sci Eng. 2018; 43: 4793–4801. doi: 10.1007/s13369-018-3121-6.
11. Sathiamurthi P, Karthi Vinith KS, Sivakumar A. Performance and emission test in CI engine using magnetic fuel conditioning with nano additives. International Journal of Recent Technology and Engineering. 2019; 8 (3): 7823–7826. doi: 10.35940/ijrte.C6213.098319.
12. Sadhik Basha J. An Experimental Analysis of a Diesel Engine Using Alumina Nanoparticles Blended Diesel Fuel. SAE Technical Paper 2014-01-1391. 2014. doi: 10.4271/2014-01-1391.
13. Sahoo RR, Jain A. Experimental analysis of nanofuel additives with magnetic fuel conditioning for diesel engine performance and emissions. Fuel. 2019; 236: 365–372. doi: 10.1016/j.fuel.2018.09.027.
14. Gumus S, Ozcan H, Ozbey M, Topaloglu B. Aluminum oxide and copper oxide nanodiesel fuel properties and usage in a compression ignition engine. Fuel. 2016; 163: 80–87. doi: 10.1016/j.fuel.2015.09.048.
15. Lenin MA, Swaminathan MR, Kumaresan G. Performance and emission characteristics of a DI diesel engine with a nanofuel additive. Fuel. 2013; 109: 362–365. doi: 10.1016/j.fuel.2013.03.042.
16. Fangsuwannarak K, Triratanasirichai K. Effect of metalloid compound and bio-solution additives on biodiesel engine performance and exhaust emissions. Am J Appl Sci. 2013; 10 (10): 1201–1213. doi: 10.3844/ajassp.2013.1201.1213.
17. Liu J, Yang J, Sun P, Ji Q, Meng J, Wang P. Experimental investigation of in-cylinder soot distribution and exhaust particle oxidation characteristics of a diesel engine with nano-$CeO_2$ catalytic fuel. Energy. 2018; 161: 17–27. doi: 10.1016/j.energy.2018.07.108.
18. Karki S, Gohain MB, Yadav D, Ingole PG. Nanocomposite and bio-nanocomposite polymeric materials/membranes development in energy and medical sector: A review. International Journal of Biological Macromolecules. 2021; 193: 2121-2139. doi: 10.1016/j.ijbiomac.2021.11.044.
19. Malakooti MH, Bockstaller MR, Matyjaszewski K, Majidi C. Liquid metal nanocomposites. Nanoscale Advances. 2020; 2 (7): 2668-2677. doi: 10.1039/D0NA00148A
20. Tetteh EK, Rathilal S. Effects of a polymeric organic coagulant for industrial mineral oil wastewater treatment using response surface methodology (RSM). Water SA. 2018; 44 (2): 155-161. doi: 10.4314/wsa.v44i2.02.
21. Ghanbari M, Mozafari-Vanani L, Dehghani-Soufi M, Jahanbakhshi A. Effect of alumina nanoparticles as additive with diesel–biodiesel blends on performance and emission characteristic of a six-cylinder diesel engine using response surface methodology (RSM). Energy Conversion and Management: X. 2021; 11: 100091. doi: 10.1016/j.ecmx.2021.100091.
22. Mahla SK, Safieddin Ardebili SM, Mostafaei M, Dhir A, Goga G, Chauhan BS. Multi-objective optimization of performance and emissions characteristics of a variable compression ratio diesel engine running with biogas-diesel fuel using response surface techniques. Energy Sources, Part A: Recovery, Utilization, and Environmental Effects. 2020: 1–18. doi: 10.1080/15567036.2020.1813847.
23. Lalhriatpuia S, Pal A. Performance and Emissions Analysis of a Dual Fuel Diesel Engine with Biogas as Primary Fuel, In: Kumar A, Pal A, Kachhwaha SS, Jain PK, editors., Singapore: Springer Singapore. 2021, 327–339. doi: 10.1007/978-981-15-9678-0_29.

 

24. Budhraja N, Pal A, Jain M, Mishra RS. Comparative Analysis of the Engine Emissions from CI Engine Using Diesel–Biodiesel–Ethanol Blends. In: Kumar A, Pal A, Kachhwaha SS, Jain PK, editors., Singapore: Springer Singapore. 2021, 363–370. doi: 10.1007/978-981-15-9678-0_32.
25. Pradeep T, GuhaRay A, Bardhan A, Samui P, Kumar S, Armaghani DJ. Reliability and Prediction of Embedment Depth of Sheet pile Walls Using Hybrid ANN with Optimization Techniques. Arab J Sci Eng. 2022; 47: 12853–12871. doi: 10.1007/s13369-022-06607-w.
26. Tayyab M, Ahmad S, Akhtar MJ, Sathikh PM, Singari RanganathM. Prediction of mechanical properties for acrylonitrile-butadiene-styrene parts manufactured by fused deposition modelling using artificial neural network and genetic algorithm. Int J Comput Integr Manuf. 2023; 36 (9): 1295-1312. doi: 10.1080/0951192X.2022.2104462.

 